ESO-TP-59

THE COME-ON-PLUS ADAPTIVE OPTICS SYSTEM: RESULTS AND PERFORMANCE

G. Rousset[1], J.L. Beuzit[2], N. Hubin[3], E. Gendron[2,4], C. Boyer[4], P.Y. Madec[1], P. Gigan[2], J.C. Richard[6], M. Vittot[6], J.P. Gaffard[4], F. Rigaut[5], P. Léna[2]

[1] ONERA, B.P. 72, 92322 Châtillon Cedex, France
[2] Observatoire de Paris, DESPA (URA 264/CNRS), 92195 Meudon, France
[3] ESO, Karl-Schwarzschild Str. 2, 8046 Garching, FRG
[4] Laserdot, Route de Nozay, 91460 Marcoussis, France
[5] CFHT, PO Box 1597, Kamuela, HI 96743, USA
[6] LEP, B.P. 15, 94453 Limeil-Brévannes Cedex, France

1. INTRODUCTION

Diffraction-limited images at infrared (IR) wavelengths were collected by the COME ON adaptive optics prototype system at the Observatoire de Haute-Provence (France) in 1989 and more recently at the ESO 3.6 m telescope (La Silla, Chile)[1,2]. They demonstrate the impressive potential of this technique for astronomy. First astronomical observations were also carried out during 1990 and 1991[3].

The COME ON PLUS system presented in this paper is an upgrade of the first prototype system. This project was completed by a collaboration between Office National d'Etudes et de Recherches Aérospatiales (ONERA), Observatoire de Paris-Meudon, Laserdot, Laboratoires d'Electronique Philips (LEP) and the European Southern Observatory (ESO). The goals were to implement an adaptive optics (AO) system dedicated to astronomy at IR wavelengths and also to prepare for the VLT program. The COME ON PLUS system was set up and tested during two technical observing runs on the ESO 3.6 m telescope in December 92 and April 93. The first astronomical observations already took place in July 93. We present here the performance measured during the laboratory tests and the first results of the technical observing runs.

2. INSTRUMENT

The main improvements brought about by this system are a better correction capability (spatial and temporal), a much higher detectivity (throughput and sensor) and a better mechanical stability for long exposure imaging. The system has already been described elsewhere[4,5,6]. The COME ON optical layout has been mainly kept[7]. Two selectable visible wavefront sensors were installed on the bench. Since April 93, a new imaging channel has been available, providing a F/45 IR focus and a standard interface for visitor instruments.

A tip-tilt mirror corrects the overall wavefront tilt fluctuations. It was not changed[7]. It has a resolution of 5 milliarcsec on the sky. This mirror now limits the correction performance of the system because of its low resonance frequencies. A new deformable mirror was manufactured by Laserdot[8]. It is a continuous facesheet deformable mirror equipped with 52 piezoelectric stacked actuators on a square array. The stroke (peak to valley) is ± 5 μm for ± 430 V.

The wavefront sensor (WFS) is a Shack-Hartmann working in the visible. It uses 32 subapertures on a 7 × 7 square grid. The field of view per subaperture is limited to 6 arcsec. The wavefront is

To be published in the Proc. ICO-16 Satellite Conf. on "Active and Adaptive Optics", Garching, Aug. 2-5, 1993

measured at a maximum rate of 200 Hz. Two WFS cameras are provided. They are selected depending on the natural guide star magnitude.

The first WFS camera is the one used in COME ON. It is a two-stage intensified Reticon array dedicated to relatively high photon flux coming from the guide star. The working visual magnitude range is m_v = 6 to 11. The photocathode is a S20 with a peak quantum efficiency of 13% at 450 nm. The P46 phosphor was chosen because of its short decay time. At low light level, this camera is read-out noise limited because of the high electronic noise level of the Reticon.

Because of this limitation, a new WFS camera was set up on COME ON PLUS in order to allow the system to work with high magnitude guide star. The camera is an Electron-Bombarded CCD (EBCCD) from LEP[9]. The photocathode is a S20R with a peak quantum efficiency of 10% at 550 nm. The gain of the tube reaches 2000 at 15 kV accelerating voltage. The CCD read-out noise was measured to 100 electrons/pixel/frame. As a consequence, this camera is always photon-noise limited. The working magnitude range on the sky was verified to be between 11 and 16, in the visible.

The observations made in order to find the limiting magnitude of the system show a large dispersion of the available photoelectrons for guide stars having the same visual magnitude as in the catalogues: this is due to the star colour. We observed 10 times more photoelectrons for a M type star (B-V colour index = 1.5) than for a A0 type star (B-V = 0). In this paper, we most often use the corrected visual magnitude of the star, which is directly related to the number of photoelectrons. When the number of photoelectrons is not known, we give the star magnitude as found in catalogues. Notice that a 15th visual magnitude star corresponds to 2.5 photoelectrons/subaperture/frame at 100 Hz.

Both adaptive mirrors are driven by a digital control loop. The real-time computer is described elsewhere[4-6]. When at high flux, the control algorithm implemented in COME ON is used[10]. For low flux, an optimized modal control algorithm was developed[4-6,11]. The modal analysis is based on a set of 52 mirror deformation modes, selected by taking into account the system configuration and the turbulence[11]. The optimized control algorithm consists in the determination of the optimum servoloop gain for each mode, i.e. their bandwidth, in terms of photon flux, r_0 (Fried parameter) and turbulence temporal behaviour. The optimum bandwidth is a trade-off minimizing the noise propagation and maximizing the turbulence correction. For each observation, we obtain a set of 52 servoloop gains. The optimized command matrix is calculated including this set of gains.

3. SYSTEM PERFORMANCE

With COME ON PLUS a significant improvement is made in terms of optical efficiency. The optical throughput of the bench was measured including all optical elements (around 10 surfaces). For the wavefront sensing channel, the throughput is 40% in the visible. For the imaging channel, the throughput is 80% in IR. This improvement was obtained by using better coatings on the mirrors.

For the servoloop bandwidth, we have to consider the two cases of low and high photon flux. For high flux, the Reticon camera is used at a frame rate of 200 Hz. Table 1 summarizes the measured bandwidths for the two axes of the tip-tilt mirror and for the deformable mirror.

	Closed-loop at -3 dB	Open-loop at 0 dB	Error at 0 dB
Deformable mirror	59 Hz	29 Hz	25 Hz
Tip-tilt mirror X axis	50 Hz	23 Hz	20 Hz
Tip-tilt mirror Y axis	57 Hz	27 Hz	23 Hz

Table 1 - Measured bandwidths on the COME ON PLUS system.

The tip-tilt mirror bandwidths are lower because of its mechanical response. For the deformable mirror, the limitations are due to the phosphor screen filtering and the high voltage amplifiers. In Table 1, we give the bandwidth of the three most important transfer functions, for comparison. The open-loop bandwidth was used in COME ON to specify the temporal response of the system. It was measured to be 9 Hz at 0 dB. But for AO, only the error transfer function bandwidth is really relevant. This bandwidth corresponds to the maximum frequency at which the AO system still brings a slight correction on the incoming wavefront. The compensated temporal spectrum of the wavefront is the product of the uncompensated spectrum by the error transfer function.

For low flux, the EBCCD camera is used. The frame rate is selected between 25 and 100 Hz. 100 Hz is the maximum frame rate in order to achieve a sufficient lifetime of the EBCCD. We consider that 10 photoelectrons/pixel/frame at 100 Hz is the maximum flux in order to ensure at least 1000 working hours at a magnitude $m_v = 11$, for average seeing conditions. With this camera, we must also optimize the bandwidth because of the photon noise level. Table 2 displays two sets of error transfer function bandwidths at -3 dB, optimized in terms of observing conditions.

Observing conditions	first order (tilts)	Second order	Lowest bandwidth
$m_v = 11$, $\overline{V} = 5$ m/s	9 Hz	7.5 Hz	4 Hz
$m_v = 15$, $\overline{V} = 17$ m/s	0.8 Hz	0.6 - 0.4	0 Hz

Table 2 - Examples of optimized bandwidths (r_0 (0.5 μm) = 20 cm).

For the 15th magnitude case, a considerable sky background was detected due to the moon. The highest bandwidths are found for the low order modes because they have the best signal to noise ratio. Note that at high flux and 100 Hz rate, the theoretical bandwidth is 11 Hz using the EBCCD camera. As shown in Table 2, the higher the guide star magnitude, the smaller the mode bandwidths and therefore smaller is the correction. This results in a relatively poor image quality as shown in the next part of this paper.

4. OBSERVING RESULTS

During the two technical runs, four different imaging cameras were used. In December 92, the IR imaging camera of COME ON was used in the J, H, K and L' bands (1.25, 1.68, 2.23 and 3.87 μm). It had a 32 x 32 array and a 0.05 arcsec pixel size on the sky. On the last night, we used an ESO 512 x 512 CCD camera in the I band (0.9 μm). The pixel size on the sky was 0.018 arcsec. In April 93, a new IR

camera was set up on the bench using the new imaging channel. It is the SHARP II camera from Max Planck Institut für extraterrestrische Physik in Garching[12]. It has a 256 × 256 NICMOS array working in J, H and K bands. In addition to this camera on the last night, an intensified CCD camera was used, working in the visible, and allowing speckle imaging with a narrow band filter.

Observations consisted generally in taking long exposure images, simultaneously with recording sets of wavefront sensor data at the sampling rate from which wavefront phases are computed. From single-star images, full width at half maximum (FWHM) and Strehl ratio (SR) are deduced. From wavefront sets, we calculate spatial and temporal properties relative to the turbulence and to the correction. In particular, r_0 (0.5 μm) and average wind speed $\overline{V}$ are estimated from the uncompensated wavefront sets.

Figure 1 displays the IR image Strehl ratio versus the Fried parameter value at the imaging wavelength. Let us first consider the high flux case. The observed Strehl ratio values (◊) are from the night of December 10 in the J, H, K and L' bands. During this night, r_0 (0.5 μm) ranged from 11 to 15 cm and $\overline{V}$ from 4 to 12 m/s. At 3.87 μm, SR is very close to 1 with an error of 10% due to a too-small camera field of view for L' images. At 2.23 μm, SR ranges from 0.8 to 0.57, at 1.68 μm from 0.26 to 0.47 and at 1.25 μm from 0.1 to 0.17. The wavefront error, estimated from the wavefront data, is of the order of 0.3 μm. This value is too low to explain the observed Strehl ratio. We suspect a static residual aberration, in the imaging path not controlled by the wavefront sensor, which limits the image quality: a triangular pattern is clearly seen on the J and H images. Another point (□) is reported corresponding to the I band observed on December 15. $\overline{V}$ is an important parameter, not shown in Figure 1, which significantly affects the image quality. Curves 1 and 2 give the theoretical behaviour of SR for 52 degrees of correction with infinite and 25 Hz bandwidth, respectively.

Let us now consider the low flux case. The observed Strehl ratio values (×,∗,+) are from a number of nights in December and April in the K and L' bands. The point dispersion is mainly due to very different turbulence conditions during these nights. This is clearly observed for the lower magnitude points (×). These points follow relatively well the behaviour of the results obtained at high flux. This is a demonstration of the quality of the control optimization. Note that under bad seeing conditions, the correction is more efficient, because for each mode, the turbulence level is significantly higher than the noise level. Considering now the increase of the magnitude for given turbulence conditions, we observe a fast decrease in the correction quality. For a 15.3 visual magnitude, SR is around 8% (r_0 (0.5 μm) = 16 cm, $\overline{V}$ = 12 m/s).

Figure 2 shows the FWHM of the images versus the wavelength (measured on the same images as Figure 1). At high flux (◊), the diffraction limit is reached down to 1.68 μm, i.e. 0.096 arcsec. In the J band (1.25 μm), the FWHM is close to the diffraction limit. In fact in this case, the partial correction profile is observed, i.e. a central core on top of a broader halo. The core is diffraction-limited and provides a 0.072 arcsec resolution. Curve 2 gives the FWHM of the seeing disk for r_0 (0.5 μm) = 15 cm. Note that 0.2 arcsec resolution is obtained in the I band. At low photon flux (×,∗,+), both the magnitude and the turbulence conditions affect the FWHM. We observe FWHM ranging from 0.13 to 0.51 arcsec in the K band.

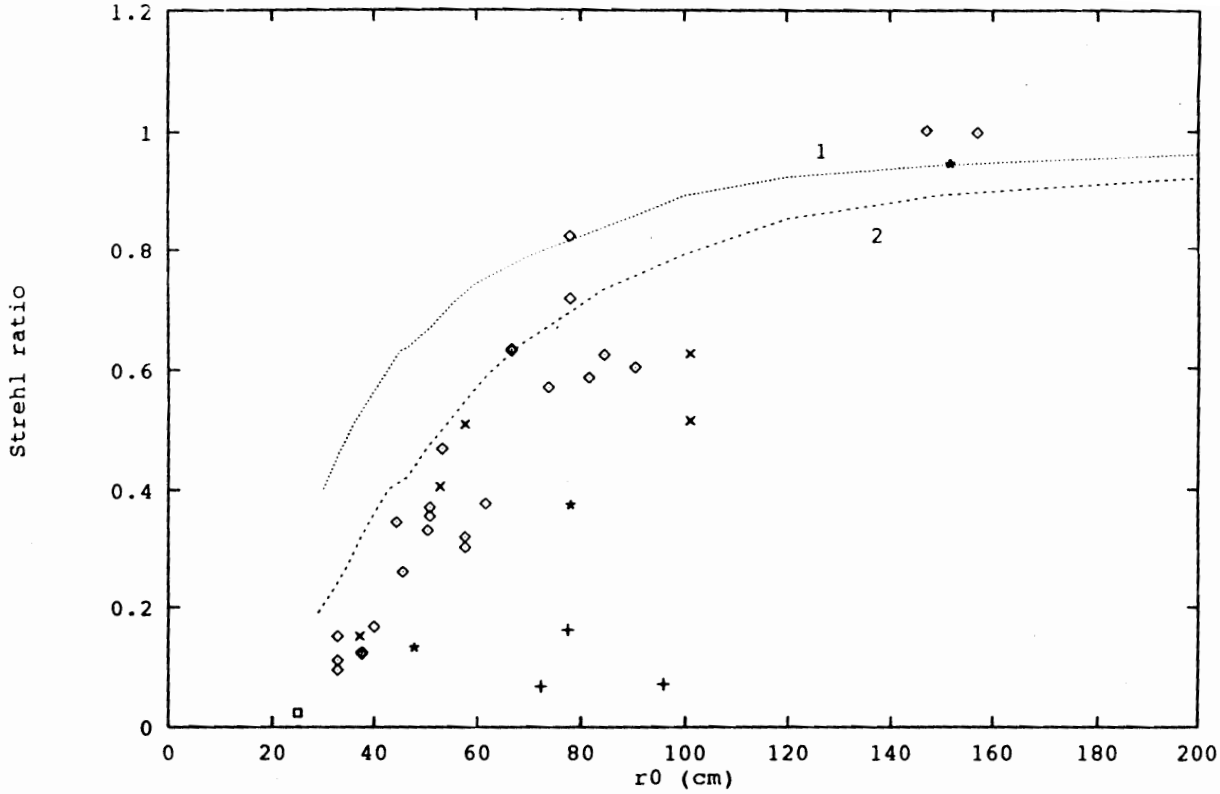

Figure 1 - Strehl ratio versus r_0 (imaging wavelength). High flux: (◇), values obtained on Dec. 10 (92) in J, H, K and L' bands (r_0 (0.5 μm) = 11 to 15 cm, $\overline{V}$ = 4 to 12 m/s); (□), values obtained on Dec. 15 in the I band (r_0 (0.5 μm) = 12 cm, $\overline{V}$ = 20 m/s); Curves 1 and 2, 52-degree-of-correction SR computed for an infinite and a 25 Hz bandwidth, respectively. Low flux: (×) visual magnitude m_v = 11 to 12, (+) $12 < m_v < 14$, (*) $m_v \geq 14$, in Dec. (92) and Apr. (93) (r_0 (0.5 μm) = 6 to 10 cm, $\overline{V}$ = 4 to 25 m/s).

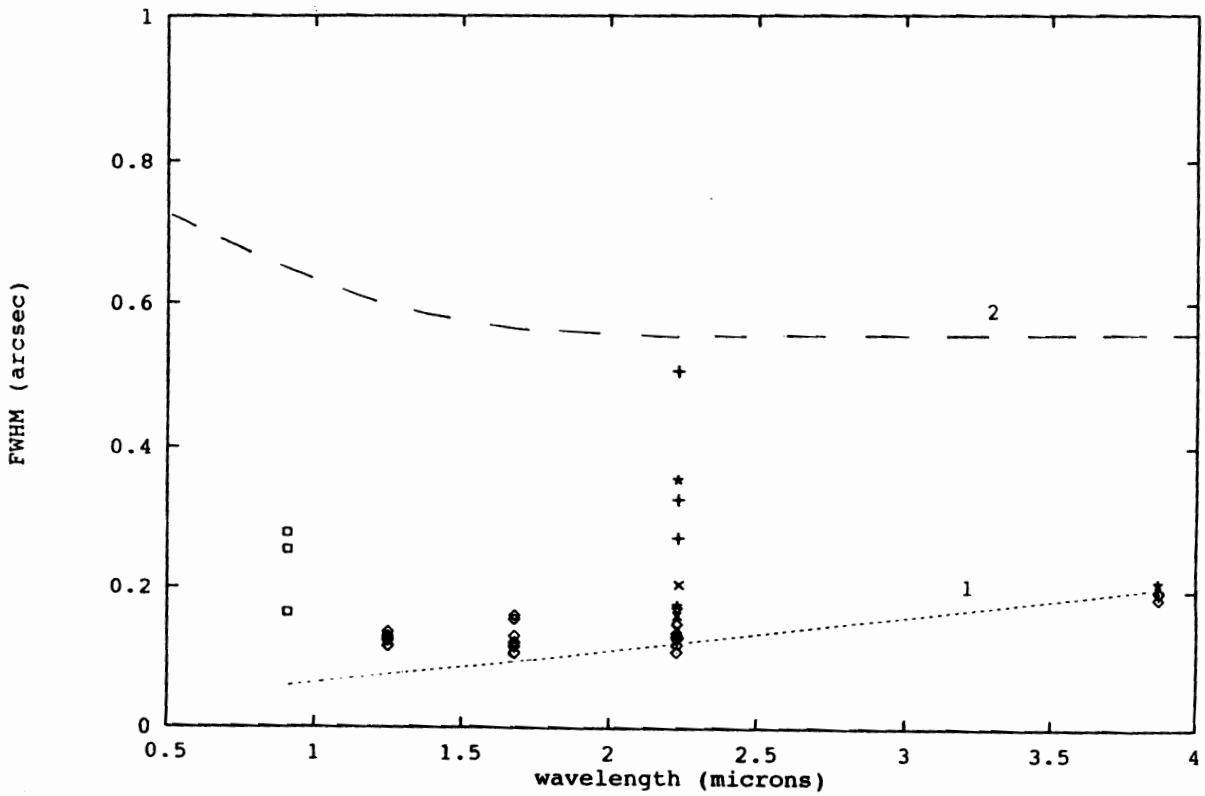

Figure 2 - FWHM versus wavelength. Curve 1: the diffraction limit. Curve 2: seeing FWHM for r_0(0.5 μm) = 15 cm. The experimental points correspond to the ones presented in Figure 1 (see caption).

In the visible (V band), the first data reductions show a gain of the order of 2 to 3 in FWHM under very bad seeing conditions ($r_0(0.5\ \mu m) = 7$ cm, $\overline{V} \geq 20$ m/s) for guide star magnitude $m_v = 11$, on April 13.

5. CONCLUSION

Let us summarize the preliminary results presented in this paper. For guide star magnitude lower than 10, i.e. at high photon flux, the best FWHM is around 0.1 arcsec and is obtained in the H and J bands. This corresponds to a full correction of the 52 modes with an error transfer function bandwidth of 25 Hz. Note that at 1.25 μm, the coherent core is observed providing a 0.072 arcsec resolution. The averaged SR is around 65% at 2.23 μm and 13% at 1.2 μm. These results could be improved by a better adjustment of the imaging path.

For guide star magnitude higher than 11, the image quality depends greatly on the number of available photoelectrons per subaperture. In these conditions, the control loop is optimized: the mode bandwidths are adjusted in order to minimize the residual wavefront error. At high magnitude for instance, the bandwidth of the low order modes can be as low as 1 Hz, and for the high orders the bandwidth tends to 0. During the two technical runs, we were able to close the loop using a guide star of visual magnitude as high as 15.7. The obtained Strehl ratio is of the order of 10% or less.

6. ACKNOWLEDGEMENTS

This project was carried out under the ESO contract 32547/TDO/90/7748 and the contract 89.R.0545 of Ministère de la Recherche et de l'Education (France). Early developments of adaptive optics components were independently supported by Direction des Recherches, Etudes et Techniques, Ministère de la Défense (France).

We are grateful to all the people involved in this project, and particularly to J.C. Fontanella and F. Merkle who initiated it. We thank Max Planck Institut für extraterrestrische Physik in Garching which implemented the SHARP II camera.

7. REFERENCES

1. G. Rousset, J.C. Fontanella, P. Kern et al., Astron. Astrophys., **230**, L29 (1990).
2. F. Rigaut, G. Rousset, P. Kern et al., Astron. Astrophys., **250**, 280 (1991).
3. F. Rigaut, M. Combes, C. Dougados et al., in Ref. 13, p. 479.
4. E. Gendron, J.C. Guby, F. Rigaut et al., Proc. SPIE **1542**, 297 (1991).
5. G. Rousset, P.Y. Madec, J.L. Beuzit et al., in Ref. 13, p. 403 and, in "Adaptive Optics for Large Telescopes Technical Digest 1992" (OSA), Vol. **19**, 106, (1992).
6. N. Hubin, J.L. Beuzit, P. Gigan et al., Proc. SPIE **1780**, 87 (1992).
7. G. Rousset, J.C. Fontanella, P. Kern et al., Proc. SPIE **1237**, 336 (1990).
8. P. Jagourel and J.P. Gaffard, Proc. SPIE **1543**, 76 (1991).
9. J.C Richard and M. Vittot, Nuclear Instruments and Methods in Physics Research, **A315**, 368 (1992).
10. C. Boyer, V. Michau and G. Rousset, Proc. SPIE **1237**, 406 (1990).
11. E. Gendron, "Modal control optimization in an adaptive optics system", in this conference.
12. R. Hofmann, M. Blietz, P. Duhoux et al., in Ref. 13, p. 617.
13. ESO Conference Proceedings n° **42**, "Progress in Telescope and Instrumentation Technologies", M.H. Ulrich Ed. (1992).